STAR Analysis Note: hadron+jet analysis in Au+Au collisions at $\sqrt{s_{\rm NN}}$=200 GeV

Thursday 14$^{\rm th}$ July, 2016

Thursday 14th July, 201615:19
— Version 2.1 —

Contents

1 Event and track selection

The base of the analysis are the Run11 $\sqrt{s_{NN}} = 200$ GeV minimum bias picoDSTs (st_physics stream) produced and stored at LBNL. The following list shows the used event and track selection cuts.

Event cuts:

- r-vertex < 2.0 cm
- |z-vertex| < 40.0 cm
- Minimum bias trigger condition used

Track cuts:

- dca < 1.0 cm
- primary particles used
- Nhitsfit > 14
- Nhitsfit/Nhitsposs > 0.52
- $p_T > 0.2$ GeV/c
- $eta < 1.0$

2 Event QA

The centrality was determined using the StRefMultCorr class. StRefMultCorr also defines the allowed z-vertex range and basic event cuts (e.g. two matched TOF hits per event). Those cuts were all applied. Figure 1 shows the vertex distribution in combinations of the x, y, and z coordinates. In all cases the r-vertex < 2.0 cm cut was already applied. The beam vertex is a bit off from zero but most events are clearly in the applied radius cut. No additional structures are found withing $|z|$ ¡ 40 cm.

Figure 2 (left) shows reference multiplicity distributions for three z-vertex ranges. A corrections for the multiplicity shift is applied, as shown on the right side of Fig. 2, during the StRefMultCorr process. The change in multiplicity is overall small as a function of the z-vertex.

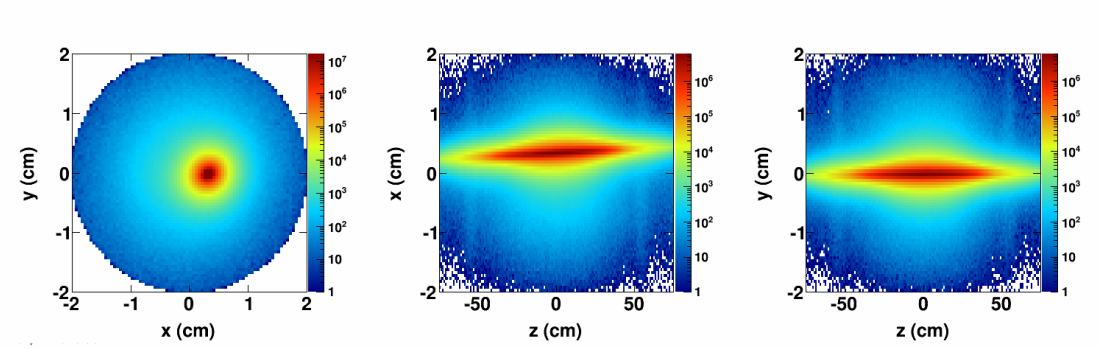

Figure 1: Event vertex distribution for (y,x),(x,z), and (y,z) after the radius cut was applied.

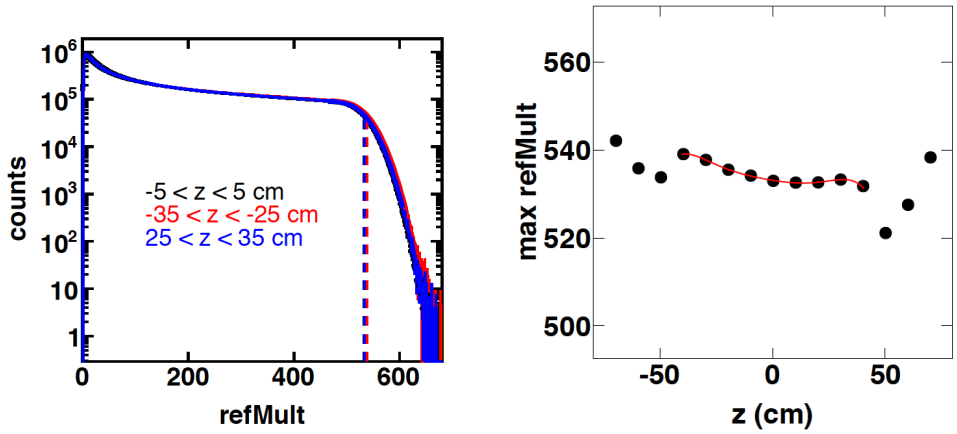

Figure 2: Left: The refmult distribution for three windows of z-vertices of the event. Right: Maximum refmult vs z-vertex position and a polynomial fit used for the StRefMultCorr correction.

Several event based QA plots are depicted in Fig. 3, 4, 5, 6. The mean reference multiplicity $< refMult >$, number of minimum bias entries per run, ZDC and BBC coincidence rates, mean vertex positions and mean number of global tracks per event are shown as a function of a run index. To select good events cuts on 2σ on the mean reference multiplicity, 2.5σ on the BBC interaction rate, and 5σ on the mean transverse momentum are applied. Removed runs are shown as red markers. Most of the dip at about 1/3 of the runs was removed by the applied selection criteria. All removed runs are listed in section 2.1.

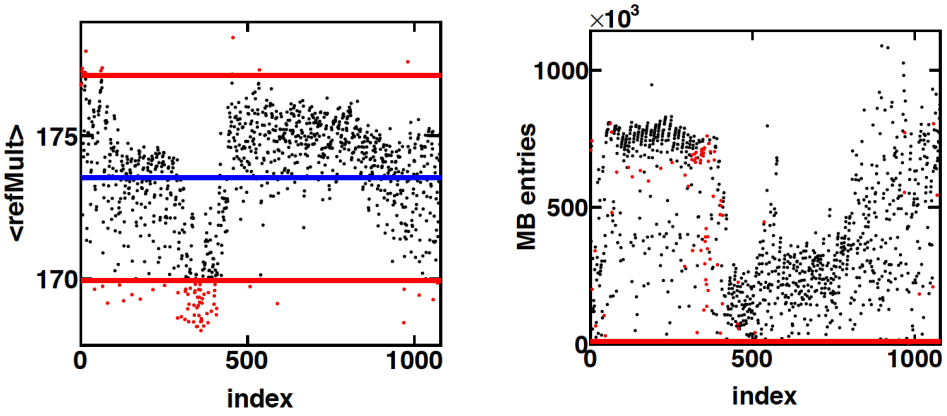

Figure 3: Left: Average refmult vs run index with selection cut on good events. Right: Number of MB events vs run index. Red symbols denote removed runs due to selection cuts.

2.1 List of bad runs excluded from analysis

12126101,12127003,12127017,12127018,12127032,12128025,12132043,12133018,12134023,
12136005,12136006,12136014,12136017,12136022,12136023,12136024,12136025,12136027,12136028,
12136029,12136030,12136031,12136034,12136054,12138017,12138021,12138081,12138082,12139006,
12139007,12139015,12139016,12139028,12139059,12139075,12139076,12139077,12139078,12139079,
12139080,12140010,12140011,12140012,12140013,12140014,12140015,12140016,12140018,12140019,
12140020,12140021,12140025,12140026,12140027,12140028,12140029,12140042,12140051,12140052,
12140053,12140054,12140055,12140056,12140064,12140066,12140067,12141001,12141002,12141003,
12141004,12141005,12141006,12141009,12141014,12141015,12141016,12141017,12141018,12141019,
12141026,12141027,12141028,12141029,12141030,12141032,12141033,12141034,12141035,12141036,
12141041,12141042,12141043,12141044,12141045,12141046,12141048,12141050,12141051,12141052,
12141056,12141059,12141060,12141061,12141062,12141063,12141064,12141065,12141066,12141067,
12141071,12141072,12142001,12142002,12142003,12142006,12142013,12142014,12142015,12142016,
12142017,12142018,12142019,12142020,12142021,12142022,12142023,12142026,12142027,12142032,
12142033,12142034,12142046,12142047,12142048,12142049,12142050,12142051,12142061,12142062,
12142063,12142076,12142077,12143016,12143018,12143054,12143075,12144001,12144002,12144013,

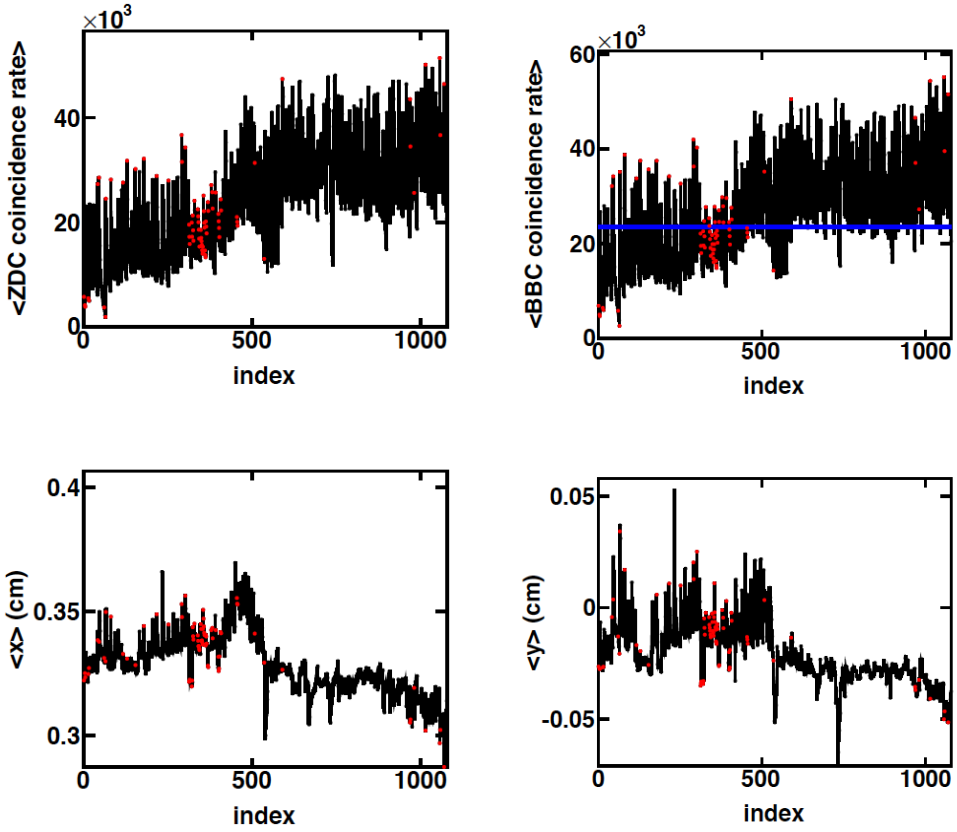

Figure 4: Upper left: ZDC coincidence rate vs run index. Lower left: Average x-vertex vs run index. Upper right: BBC coincidence rate vs run index. Lower right: Average y-vertex vs run index. Red symbols denote removed runs due to selection cuts.

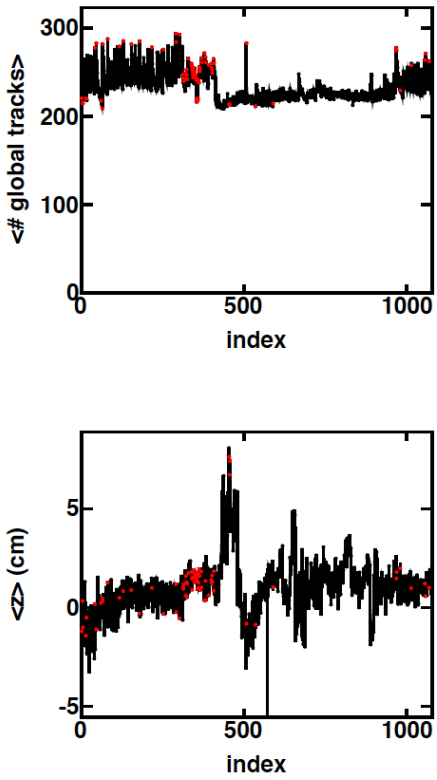

Figure 5: Top: Average number of global tracks vs run index. Bottom: Average z-vertex vs run index. Red symbols denote removed runs due to selection cuts.

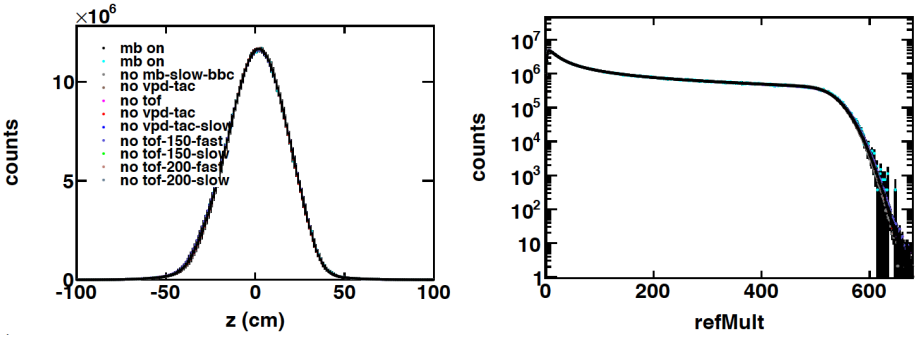

Figure 6: Left: z-vertex distribution for different trigger conditions. Right: Refmult distribution for different trigger conditions.

12144014,12144027,12144028,12157038,12157051,12158040,12158041,12158054,12158056,12158057,
12162055,12162056,12162057,12162058,12164037,12164078,12164079,12166002,12166003,12167015,
12167024,12167052,12168002,12168009,12168022,12168077,12170044,12170045,12170054,12170056

3 Code description

In the following the analysis chain is explained. The actual analysis uploaded to CVS starts with the third item.

- LBNL Run11 minimum bias (st_physics stream) picoDSTs are used as input

- New jet trees are produces (Analysis_Snurf.*). The classes are StJetTrackEvent and StJetTrackParticle which contain the basic event information (refmult, etc.) and charged particle information (mass, TLorentzVector, charge, etc.).

- The main jet analysis is performed with StJetAnalysis.* (JetAnalysis_Macro.cc). The first step is to subdivide the jet trees into the 640 event classes (20 z-vertex bins, 8 centrality bins, 4 event plane bins). This is done separately for central (0-10%) and peripheral events (60%-80%). This is needed for the mixed event procedure. Then the mixed event trees are produced. The jet reconstruction is finally done on the same event and mixed events. Also the efficiencies, response matrices, and PYTHIA embedding calculation are done in this code. The output are various histograms which are analyzed in macros.

- ReCoil_Jet_Ana_histo.cc: The main macro which is doing mixed event normalization and subtraction for 1D and 2D histograms. It also creates the jet area histograms. A pre-comparison to PYTHIA is also done.

- Plot_eta_phi.cc is plotting the η vs. ϕ track distribution for same event and mixed event.

- PlotJets2D.cc is plotting the η vs. ϕ jet event display.

- RefMult_Jet_Ana.cc is plotting the refmult distribution.

- Eff_Sim.cc is a small Monte Carlo macro to study the effect of an efficiency dip in the acceptance.

- Plot_sigma.cc is analyzing the 2D (jet p_T vs. $\Delta\phi$) histograms. It is also plotting the ρ distributions.

- Jet_unfold_ratio.cc is analyzing the unfolded spectra (selecting the spectra, calculating systematic error bars, calculating the I_{AA}).

- Jet_radii_ratio.cc is calculating ratios of different jet radii plus corresponding errors.

- Jet_systematic_err.cc is calculating a part of the systematic errors listed in the systematic error table.

- Jet_data_unfold.cc and Execute_Jet_data_unfold.C are doing the unfolding for test purposes. It also produces the δp_T figures. The real unfolding is done in a different code described below.

- StJetUnfold.* (Jet_data_unfold_Macro.cc) is performing the main unfolding and systematics.

4 Mixed event subtracted spectra

The ME procedure generates an event population without multi-hadron correlations, but with the detailed features of real data in terms of non-uniformity in instrumental response and variation in detector acceptance due to the $z_{\rm vtx}$ distribution. Incorporation of such detector effects in the ME population is needed for accurate determination of the uncorrelated background distribution in the recoil jet population.

In the ME procedure events are assigned to exclusive classes, with each class corresponding to a narrow bin in M, the uncorrected charged particle multiplicity; $z_{\rm vtx}$, the z-position of reconstructed vertex; and φ_{EP}, the azimuthal orientation of the event plane (EP) in the laboratory frame. There are 8 bins in M, 20 bins in $z_{\rm vtx}$, and 4 bins in φ_{EP}, corresponding to 640 distinct event mixing classes. Within each multiplicity bin the distribution of track multiplicity is sampled from the SE dataset, to accurately reproduce the multiplicity distribution of real events. This procedure accounts for the multiplicity bias in events containing a high-$p_{\rm T}$ trigger hadron, relative to the MB population.

A mixed event with M tracks is generated by drawing one track from each of M different real events. For efficient construction of ME events, the event mixing algorithm draws from a buffer of about 1000 real events, with the algorithm terminating when any event in the buffer has had all its tracks used. All unused tracks remaining in the buffer are discarded, the event buffer is refilled, and the

procedure is repeated. Tracks are therefore used at most once in the mixing procedure.

The jet distribution due to uncorrelated background is determined by carrying out the same jet reconstruction procedure on the ME events as is used for the real data. No high-p_{T} trigger hadron is required; the trigger axis from ME events is chosen by selecting a random track, resulting in a similar azimuthal distribution to that of the SE population.

The mixed event subtracted spectra for all jet radii are shown for central events in Fig. 7 and for peripheral events in Fig. 8. We already compare the spectra to PYTHIA before unfolding by smearing the detector level PYTHIA spectra with δp_T. A good agreement in spectral shape and magnitude is observed for peripheral events, while central events show a significant difference, most likely due to jet quenching.

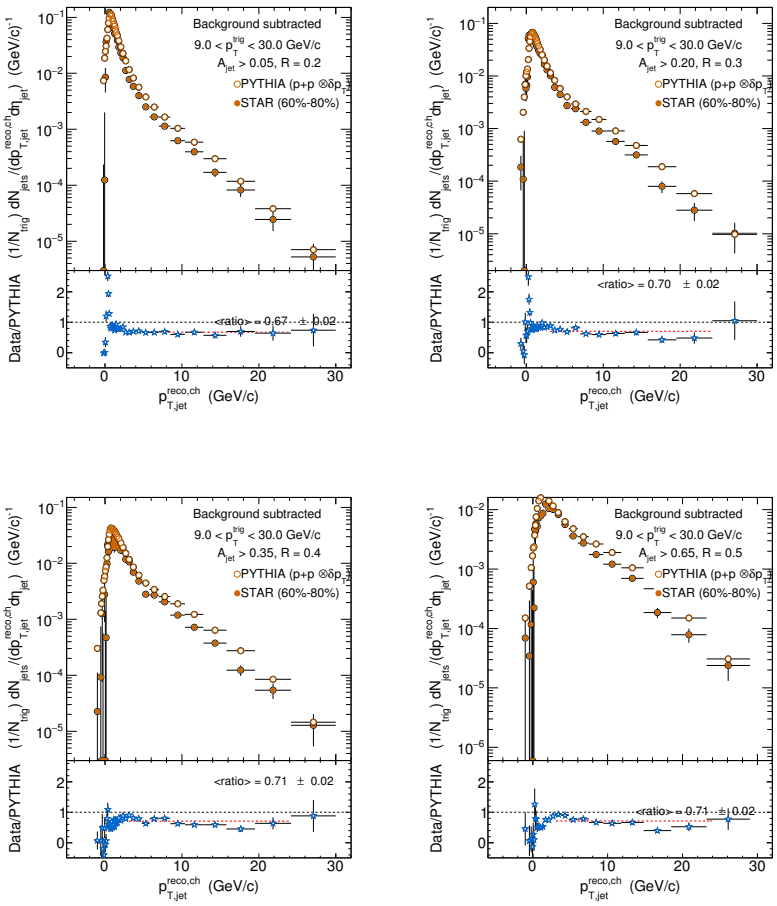

Figure 7: Mixed event background subtracted raw recoil jet spectra in comparison to PYTHIA$\otimes\delta p_T\otimes$eff. for central collisions for R = 0.2-0.5.

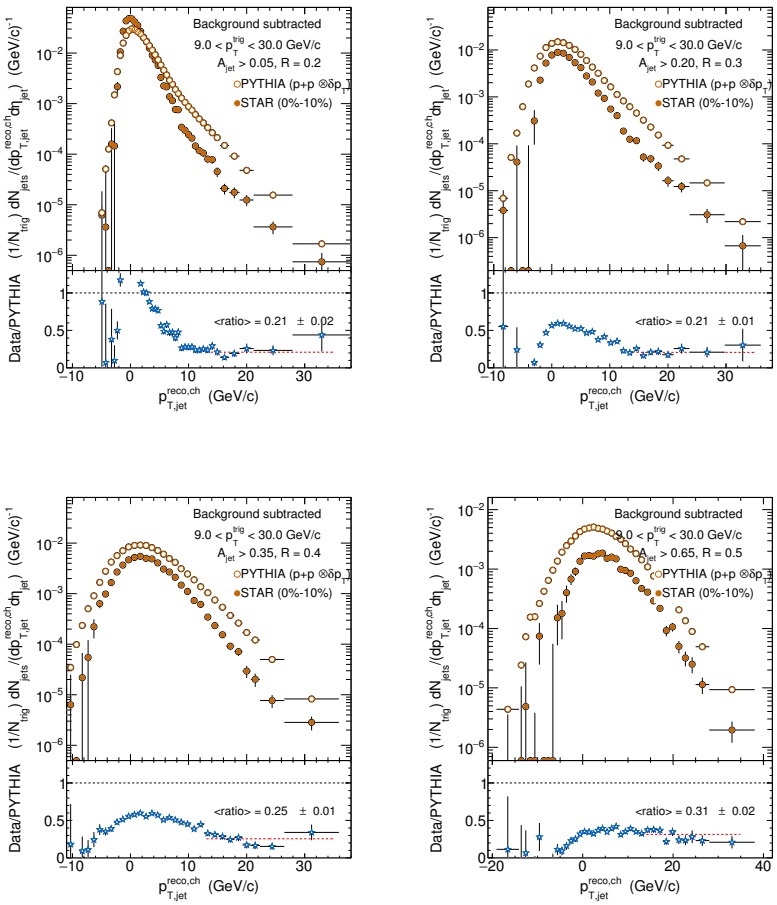

Figure 8: Mixed event background subtracted raw recoil jet spectra in comparison to PYTHIA$\otimes\delta p_T\otimes$eff. for peripheral collisions for R = 0.2-0.5.

5 Jet area distributions

All jet area distributions for same event and mixed event for all four radii are shown in Fig. 9 and 10. There is an overall agreement between same event and mixed event, which indicates that the distributions are mainly driven by a combination of the jet finding algorithm and acceptance. The applied jet area cuts are shown as vertical dashed lines.

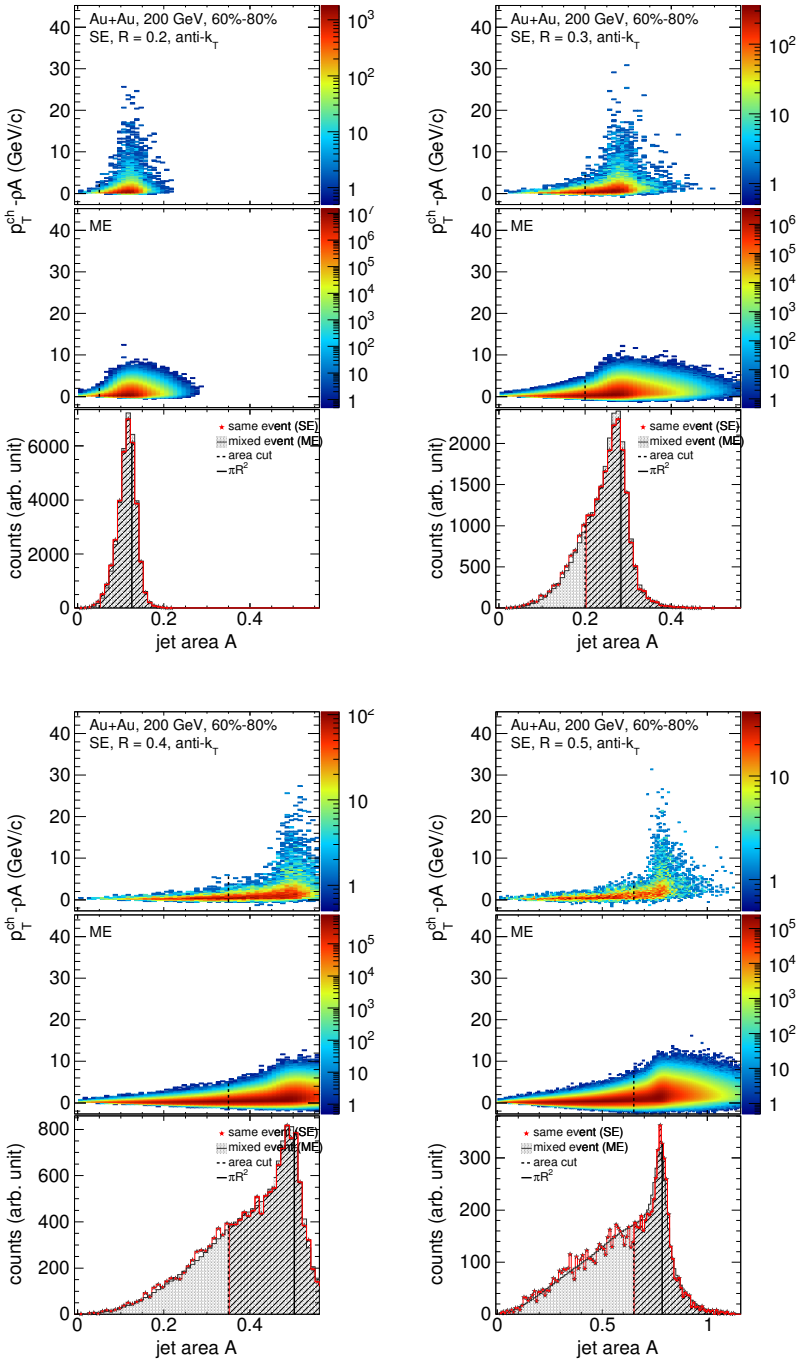

Figure 9: Recoil jet p_T vs jet area for R=0.2-0.5 for 60%-80% collisions.

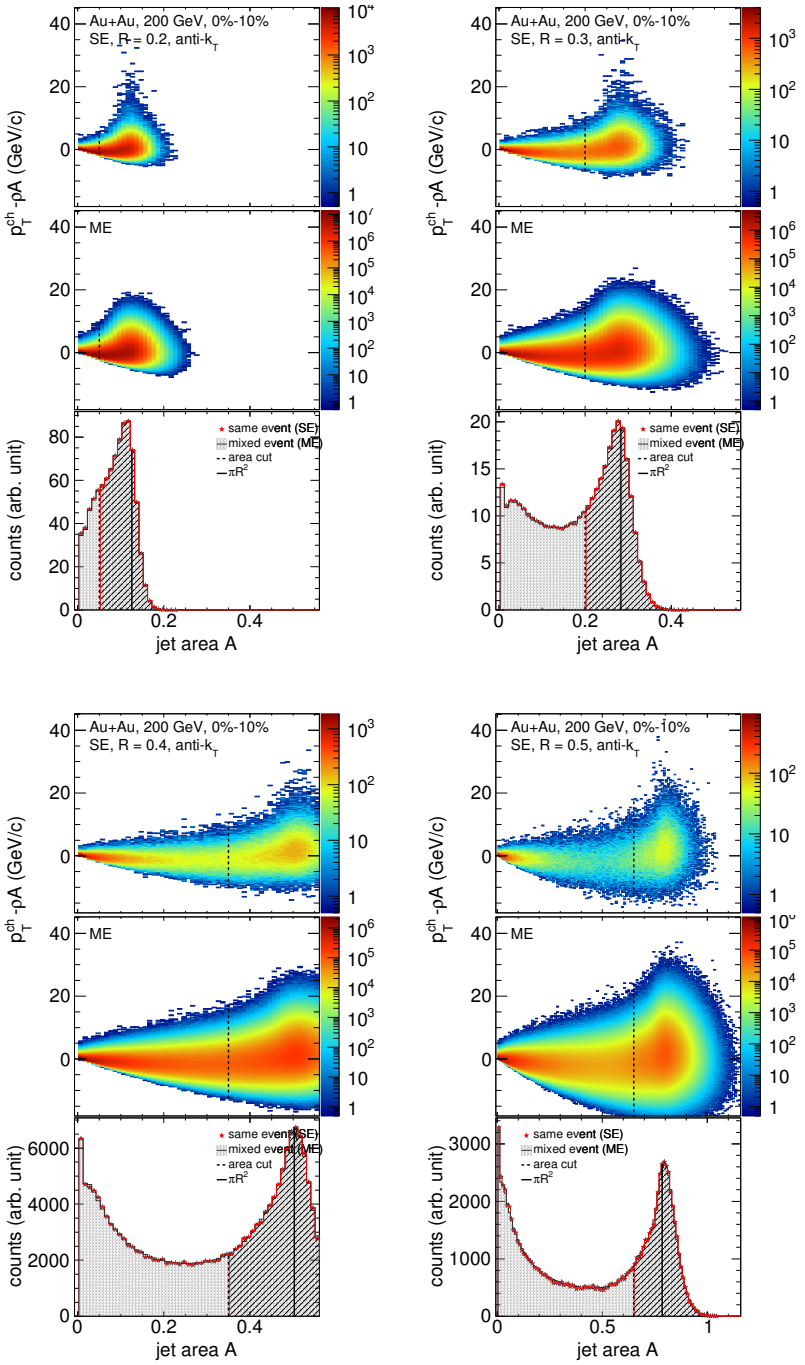

Figure 10: Recoil jet p_T vs jet area for R=0.2-0.5 for 0%-10% collisions.

6 Jet reconstruction efficiency

The matching procedure between particle-level and detector-level jets described in the paper does not generate a match for every particle-level jet. The corresponding detector-level jet can be lost due to the jet area cut; fiducial cuts; or instrumental response, for instance loss of tracks carrying a large fraction of the jet energy. The jet area cut generates a small inefficiency for $p_{\mathrm{T,jet}}^{\mathrm{part}} < 4$ GeV/c, with negligible effect at larger $p_{\mathrm{T,jet}}^{\mathrm{part}}$.

Figure 11 shows for all radii the jet matching/reconstruction efficiencies based on a PYTHIA study. Only R = 0.3 is shown in the paper.

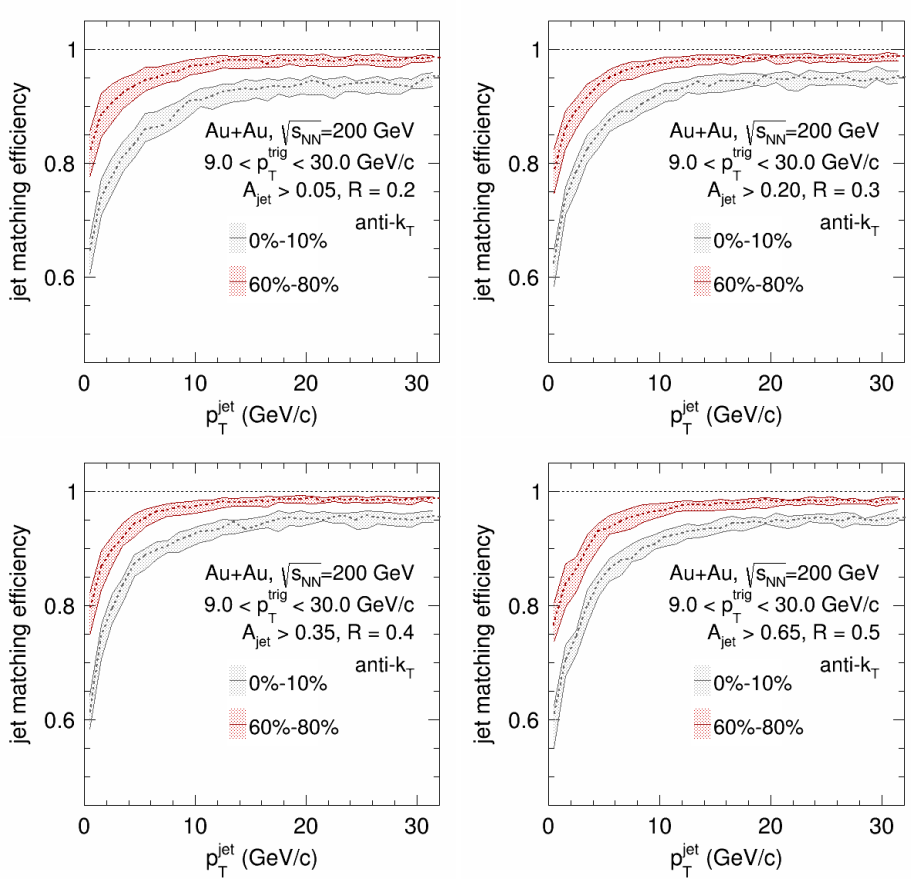

Figure 11: Matching efficiency for peripheral and central collisions as a function of jet transverse momentum for R = 0.2-0.5.

7 Mixed Event subtraction

Figure 12 is showing the details of the low p_T part of the R = 0.2 and R = 0.5 spectra after mixed event subtraction. Some entries are negative (by definition based on the normalization) but mostly in agreement (within 1 σ uncertainties) with 0. The unfolding procedure will treat them as 0 values with little to no impact on the unfolded spectrum.

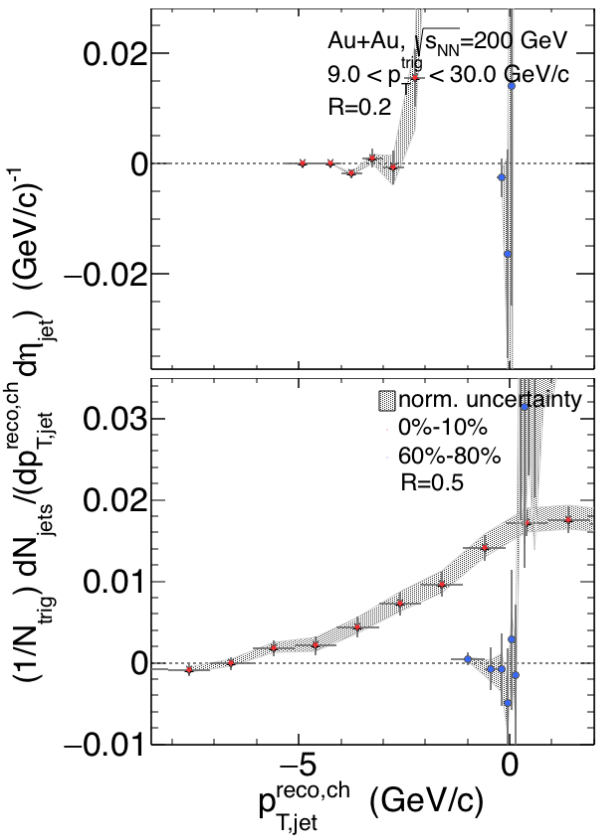

Figure 12: Zoom in to the low p_T part of the mixed event subtracted spectra. The yield is generally in agreement with 0 within uncertainties.

8 Unfolding

The mixed event subtracted jet distributions must be corrected for the effects of local fluctuations in background energy density and for instrumental response. The corrections are carried out using regularized unfolding methods. In this approach, the measured jet distribution M and true jet distribution T are related by a response matrix,

$$M(p_{\mathrm{T,jet}}^{\mathrm{det}}) = R_{\mathrm{tot}} \left(p_{\mathrm{T,jet}}^{\mathrm{det}}, p_{\mathrm{T,jet}}^{\mathrm{part}} \right) \times T(p_{\mathrm{T,jet}}^{\mathrm{part}}), \tag{1}$$

where R_{tot} is the cumulative response matrix, encoding both background and instrumental response effects; $p_{\mathrm{T,jet}}^{\mathrm{part}}$ is the particle-level charged-jet p_{T}; and $p_{\mathrm{T,jet}}^{\mathrm{det}}$ is the detector-level or reconstructed jet p_{T}. We assume that R_{tot} can be factorized as the product of the response matrices for instrumental response R_{det} and background fluctuations δp_{T}, and determine these two component independently. The factorization approximation was studied in simulations and found to be accurate.

The corrected spectrum, which is a measurement of T, is determined by inverting Eq. 1. However, exact inversion of Eq. 1 can result in a solution which has large fluctuations in central values and large variance, due to statistical noise in $M(p_{\mathrm{T,jet}}^{\mathrm{det}})$. A physically interpretable solution is obtained by regularized unfolding, which imposes an additional smoothness constraint on the solution.

The unfolding procedure is described in detail in the paper. We are using Bayesian and TSVD unfolding. As a prior either a Levy function with two parameter or PYTHIA (with additional suppression factor) is used. All parameters are varied in 2-3 steps. In addition we used three different mixed event normalizations. The regularization parameter k has values between 1 and 5. Once an unfolding with a certain k-value fullfills the χ^2 criteria all larger k-value solutions are skipped. Larger k-values increase the unfolding error bars but usually do not improve the central value solution much more.

Figure 13 shows exemplarily the unfolding matrices for central Au+Au collisions for R=0.3 jets in the binning used for the unfolding procedure. The lower plots is the product as finally used.

Unfolding examples for R = 0.2, 0.3, 0.4, and 0.5 are shown for central events in Fig. 14, peripheral event in Fig. 15 and only for R = 0.3 in Fig. 14. The header gives information about the used prior (PYTHIA or Levy function) and the unfolding method (Bayesian or Levy) and the use regularization parameter kreg. Not all details are listed, e.g. used normalization, used δp_T method etc.

Table 8 shows the number of accepted priors for each centrality and jet radius. Usually a factor two more priors were used as input. The selection is based on the backfolding χ^2 relative to data. The χ^2 in the figures is per ndf but does not include the errors from the backfolded distribution due to a strong correlation, only the statistical errors from data is compared to the central values of the backfolded distribution.

All accepted unfolding solutions are used to calculate the systematic error bar. Latter one is defined as the envelope of all solutions.

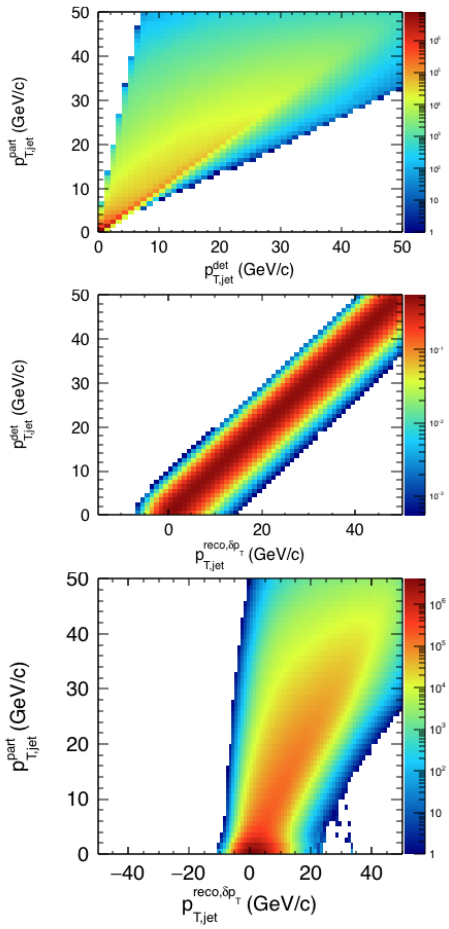

Figure 13: (Color online) Upper: instrumental response matrix $R_{\rm det}$ for central Au+Au collisions for R=0.3 jets. Middle: Uncorrelated background response matrix $\delta p_{\rm T}$for central Au+Au collision for R=0.3 jets. Lower: Product of the upper two matrices.

R	0.2	0.3	0.4	0.5
0%-10%	45	181	312	270
60%-80%	39	137	267	162

Table 1: Number of priors used for all four jet radii.

The individual unfolding solution are shown in Fig. 17 for all four radii. Figure 18 shows the effect of the $\pm 5\%$ track reconstruction efficiency variation on the spectra.

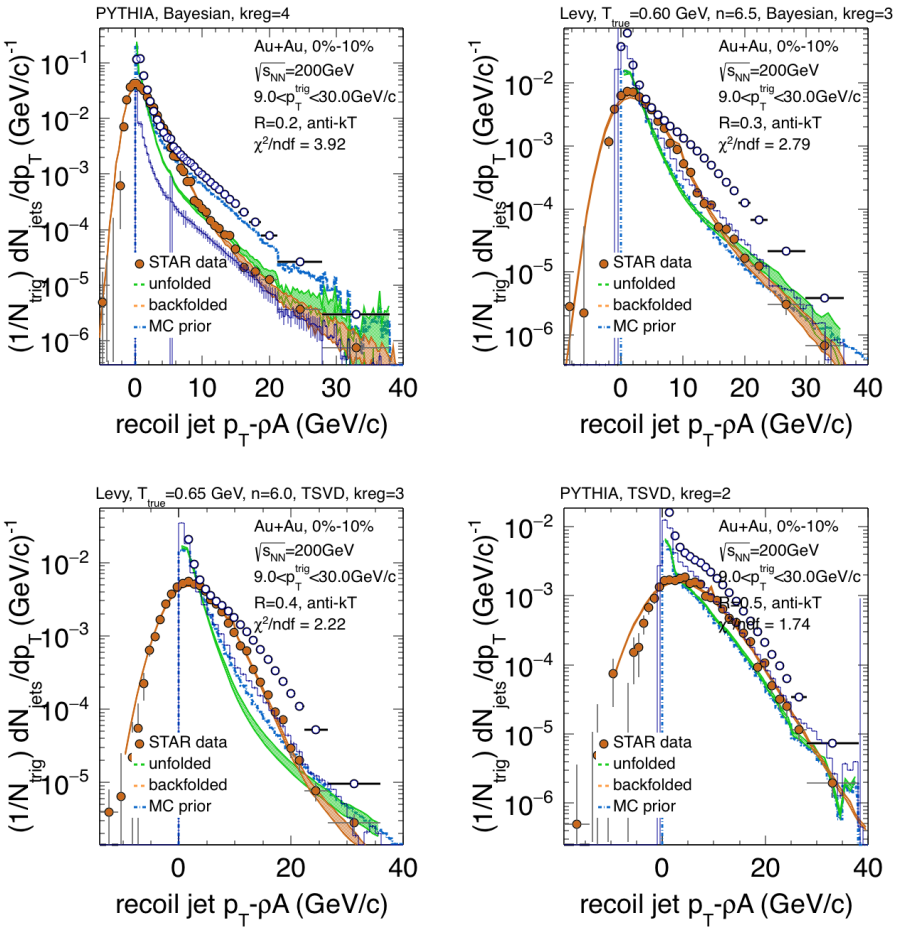

Figure 14: Unfolding examples for R = 0.2, 0.3, 0.4, and 0.5 for central events. The header gives information about the used prior (PYTHIA or Levy function) and the unfolding method (Bayesian or Levy) and the use regularization parameter kreg.

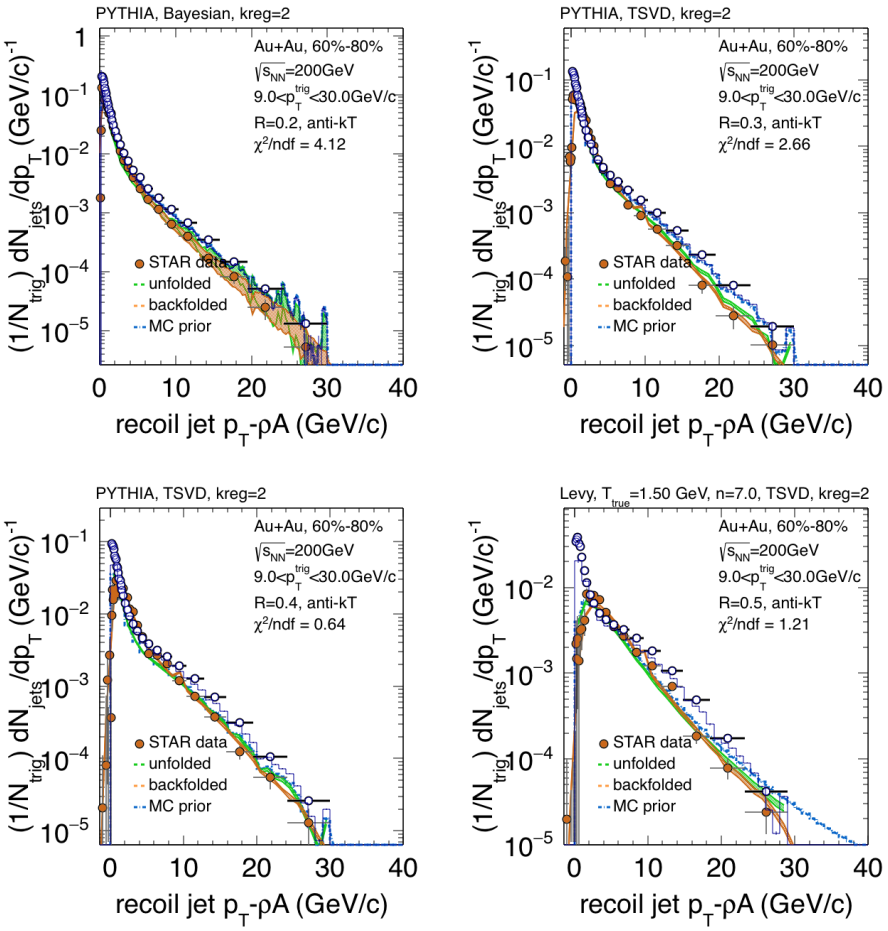

Figure 15: Unfolding examples for R = 0.2, 0.3, 0.4, and 0.5 for peripheral events. The header gives information about the used prior (PYTHIA or Levy function) and the unfolding method (Bayesian or Levy) and the use regularization parameter kreg.

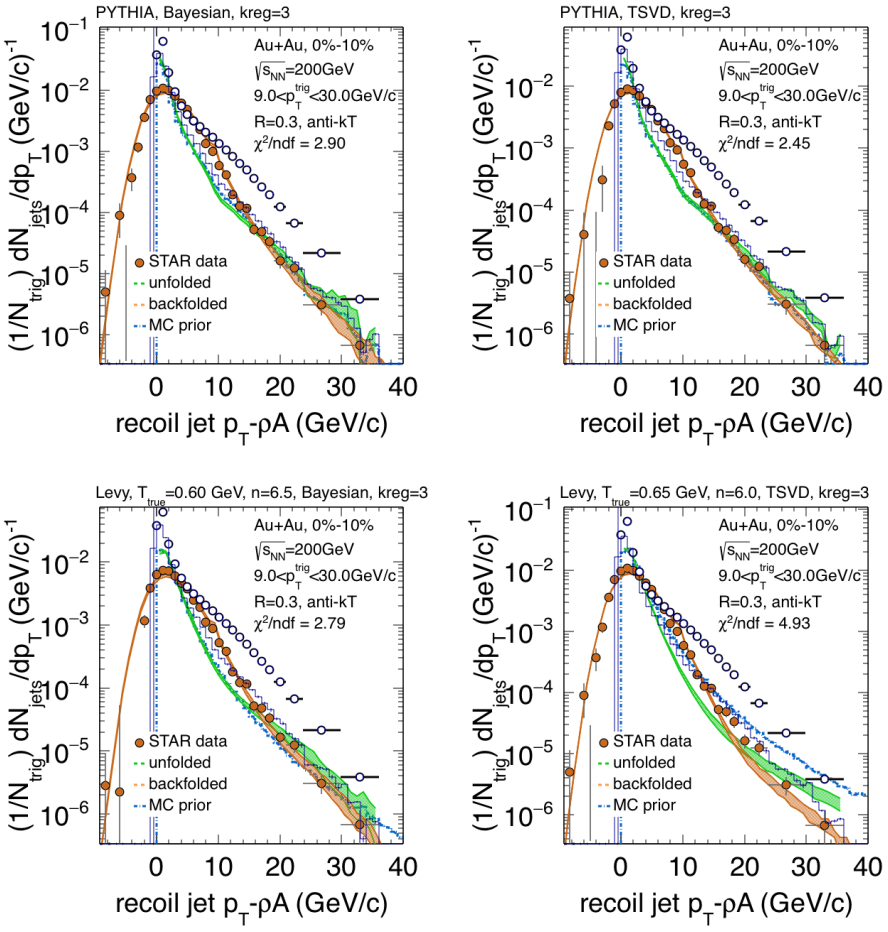

Figure 16: Unfolding examples for R = 0.3 for central events. The header gives information about the used prior (PYTHIA or Levy function) and the unfolding method (Bayesian or Levy) and the use regularization parameter kreg. Different variation for the unfolding are shown. The lower right spectrum was not accepted due to large χ^2.

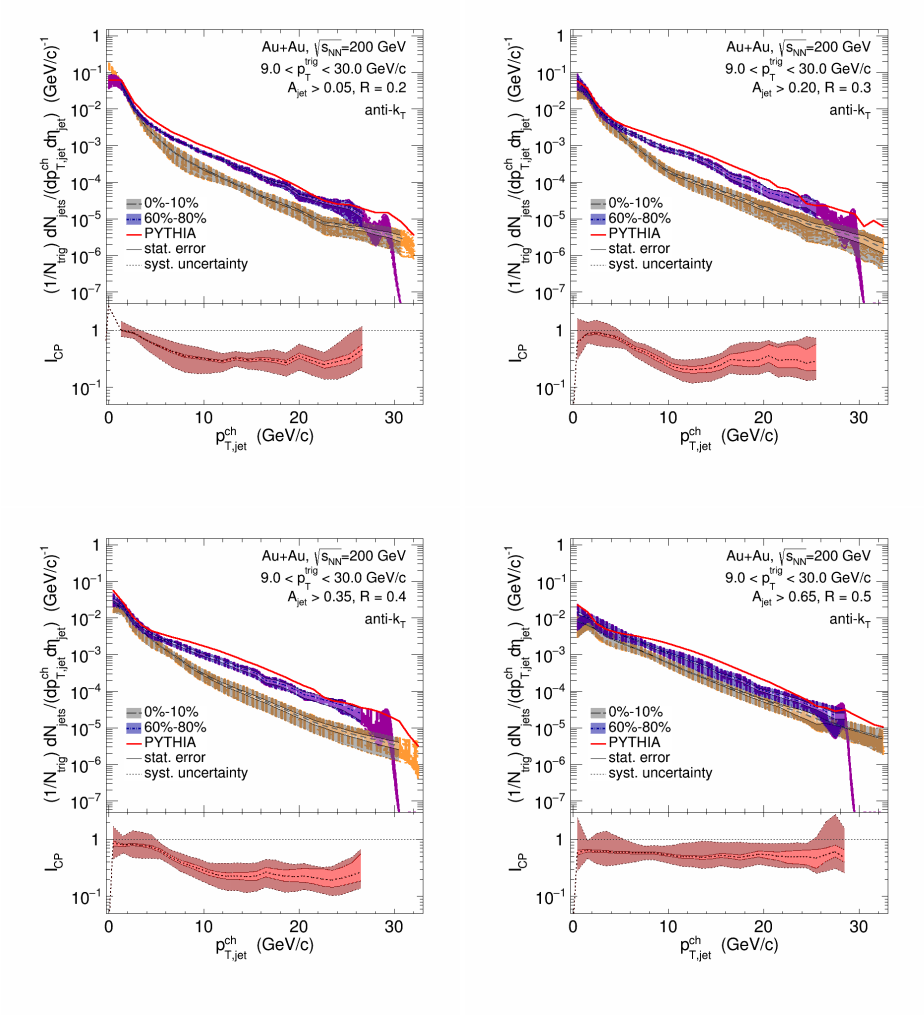

Figure 17: Unfolded recoil jet spectra for R = 0.2-0.5 for central and peripheral collisions. The individual lines within the systematic error band show all evaluated systematics (priors, normalization, δp_T, etc.).

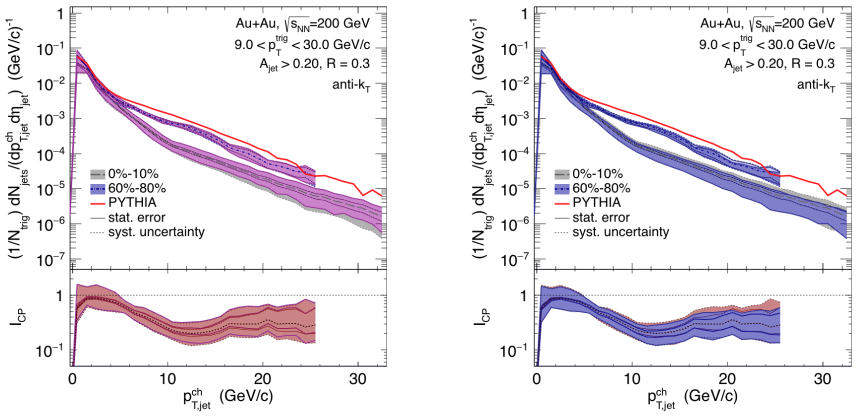

Figure 18: Unfolded recoil jet spectra for R = 0.3 for central and peripheral collisions. The left plot shows in magenta the unfolded spectrum for a tracking efficiency of 0.95 relative to the nominal efficiency, the right plot shows in blue the unfolded spectrum for a tracking efficiency of 1.05 relative to the nominal efficiency.

9 Jet Energy Resolution (JER)

Figure 19 is showing the reconstructed and matched detector level transverse momentum for five input jet momenta. We have fitted the main peak of each distribution with a Gaussian. This width corresponds mainly to the momentum resolution effects, whereas the tail corresponds to the loss due to track reconstruction efficiency. The RMS over input energy is a quantitative measure of the jet energy resolution.

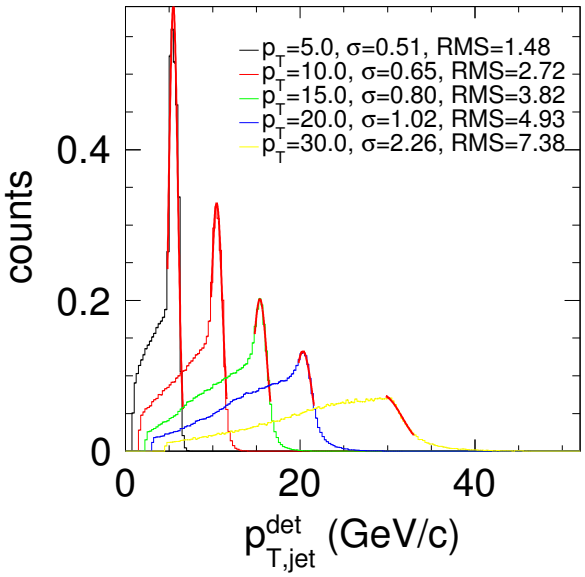

Figure 19: The reconstructed and matched detector level transverse momentum for five input jet momenta. The width (σ) is resulting from a Gaussian fit to the main peak, the RMS is for the whole distribution.

10 $\Delta\phi$ dependent normalization of mixed event

Figure 20 (left) show the same event and mixed event yields in the normalization region as a function of the $\Delta\phi$ angle between trigger particle and recoil jet for R = 0.3 and central events. Right: Ratio of same event over mixed event for the three normalizations. The normalization variation was done using the 1D scaling factors (three normalization ranges) since a $\Delta\phi$ dependent bin-by-bin scaling for three normalization ranges would introduce too many fluctuations. The 1D (global) scaling factors were applied on the $\Delta\phi$ dependent mixed event yields.

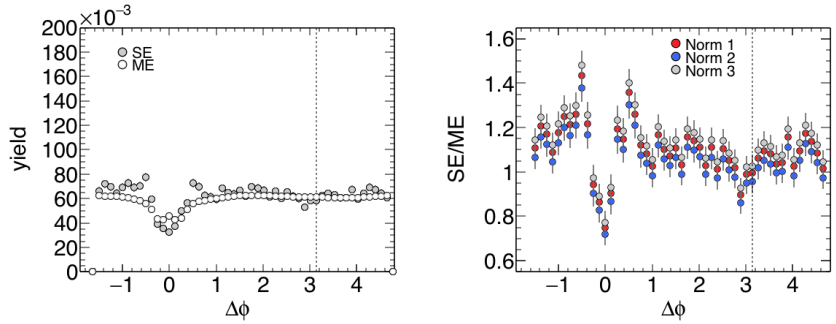

Figure 20: Left: Same event and mixed event yields in the normalization region as a function of the $\Delta\phi$ angle between trigger particle and recoil jet for R = 0.3 and central events. Right: Ratio of same event over mixed event for the three normalizations (see text for details).

11 Monte Carlo efficiency study

We studied the effect of a not flat track reconstruction efficiency as a function of the azimuthal angle ϕ. Figure 21 shows results of a Monte Carlo study. A jet p_T was sampled from a Levy function (red curve in upper right figure). The jets were randomly, with a maximum value of 8, split into tracks, distributed within R = 0.3 in ϕ. Efficiencies (upper left figure) were applied to those tracks based on an averaged efficiency curve and a more realistic one with a dip as observed in the run11 data. The resulting the jet p_T spectra are shown in the upper right figure. The ratio in the lower left figure shows no significant difference. Therefore a combined unfolding with an averaged efficiency can be used.

Figure 22 is showing the same calculation except that the dip is now wider and deeper. A clear distortion is observed in the ratio. For such cases one would need to use a different unfolding procedure.

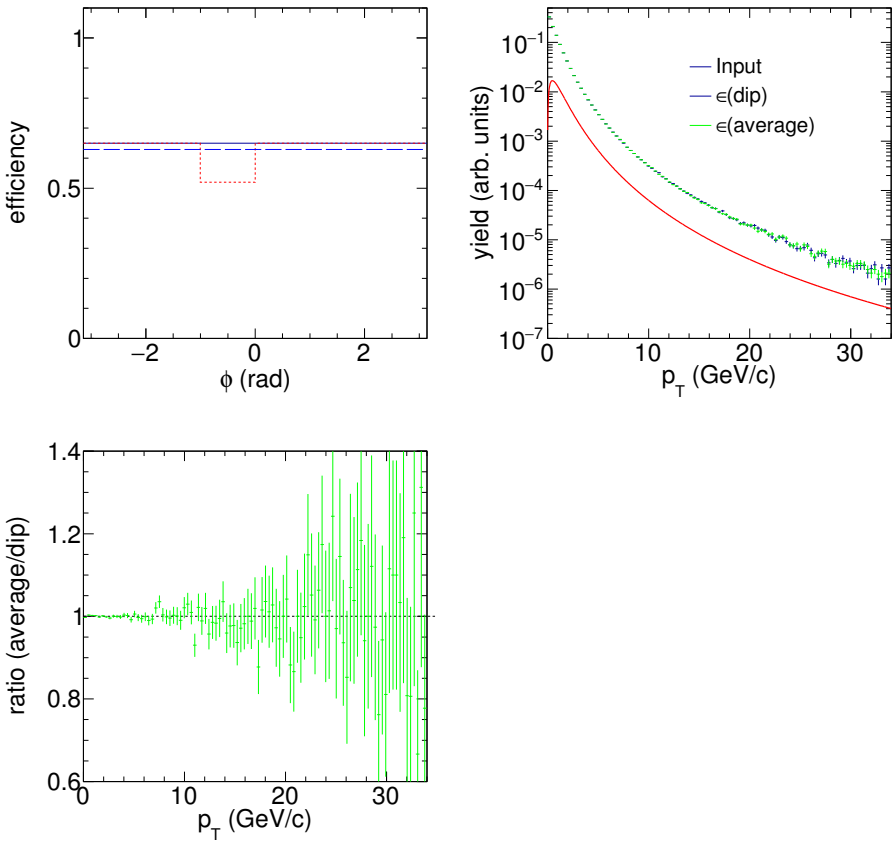

Figure 21: Monte Carlo study on the effect of a realistic dip in the reconstruction efficiency (see text for details). Top left: Realistic efficiency as a function of the azimuthal angle ϕ (red) and an averaged efficiency (blue dashed). Top right: Input p_T distributions for jets (red) and reconstructed spectra for the two efficiencies. Lower left: ratio of the two jet spectra.

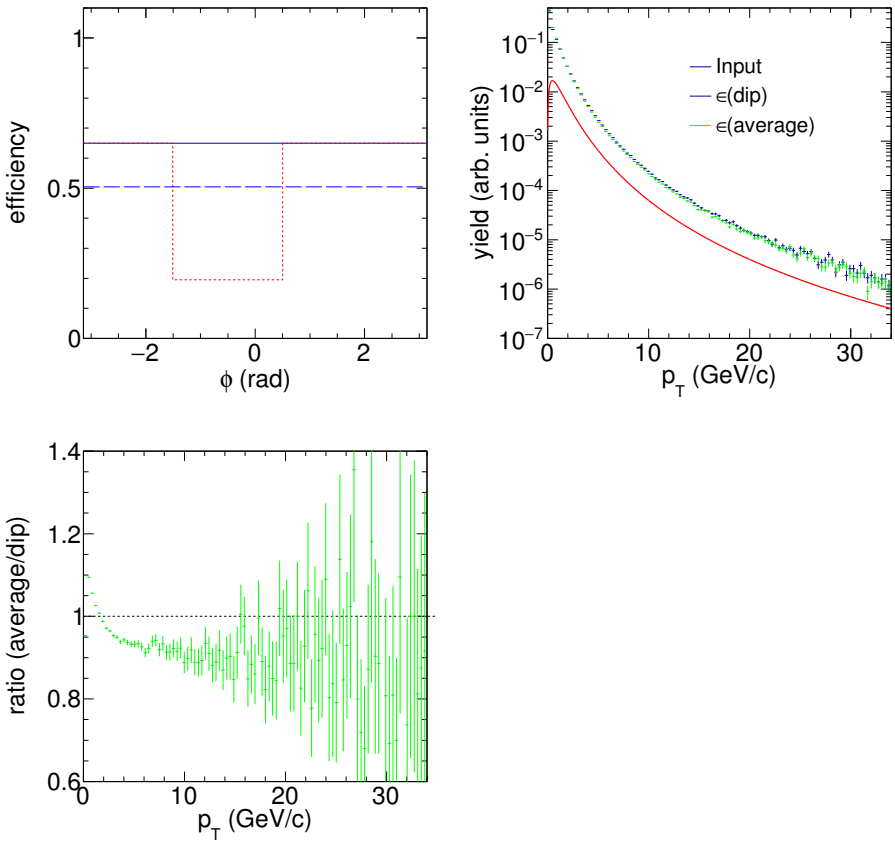

Figure 22: Monte Carlo study on the effect of a extreme dip in the reconstruction efficiency (see text for details). Top left: Realistic efficiency as a function of the azimuthal angle ϕ (red) and an averaged efficiency (blue dashed). Top right: Input p_T distributions for jets (red) and reconstructed spectra for the two efficiencies. Lower left: ratio of the two jet spectra.

12 Difference between trigger axis and jet axis

Figure 23 shows the difference in azimuthal angle between a trigger particle with p_T >9 GeV/c and its jet from PYTHIA events. The jet cone radius was R = 0.3.

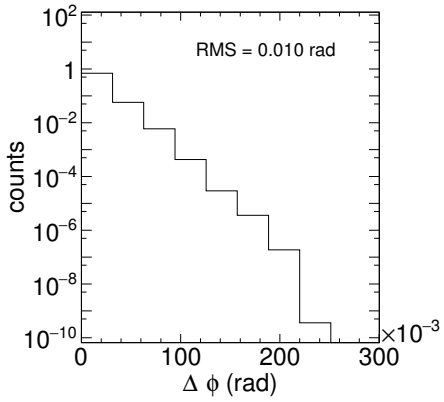

Figure 23: The difference in azimuthal angle between a trigger particle with p_T >9 GeV/c and its jet from PYTHIA events.

13 NLO Calculations

Parton level h-jet distributions are calculated using pQCD at NLO based on the code developed by Daniel De Florian. The response matrix between parton-level and charged particle-level jets is generated based on PYTHIA (6.4.26, Perugia-0 tune). The systematic uncertainty is about 30-40%, due mainly the variations of the renormalization and factorization scales. Below the setting for the calculations:

- Trigger: $9 < p_T^{hadron} < 30$ GeV/c
- $|\eta_{hadron}| < 0.9$
- Jets: anti-k$_T$, R = 0.2-0.5
- $|\eta_{jet}| < 0.5$
- $|\Delta\phi_{h,jet}| < 0.6$

- PDF: CT10 NLO, (CTEQ6M and MRST2002 for systematic errors)

- FF: DSS

- Scale: p_T^{hadron} is used for the trigger hadron cross section

- Scale: $(p_T^{hadron} + p_T^{jet})/2$ is used for calculating the cross section of the h-jet coincidence rate

Renormalization scale	initial state factorization scale	final state factorization scale
1	0.5	0.5
1	2	2
0.5	1	1
2	1	1

Table 2: Combinations of scale uncertainties used for the NLO systematic uncertainty evaluation.

Three PDFs (see item list) and various combinations of scale uncertainties are used (see Table 13) to evaluate the systematic uncertainties for the NLO calculations. Figure 24 shows examples of the response matrix, correction factors, systematic uncertainties, and the final spectra.

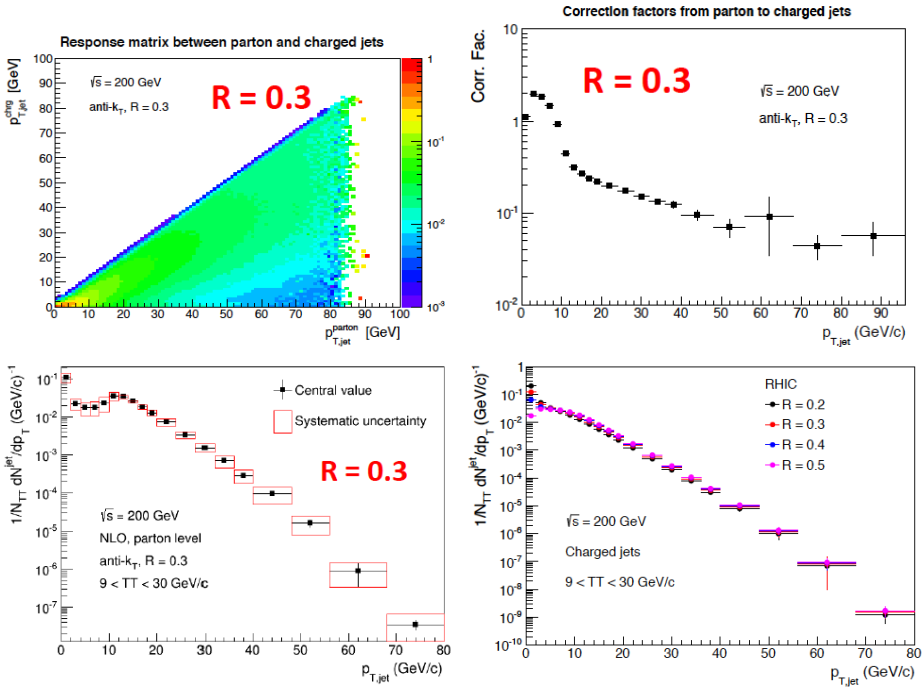

Figure 24: Top left: Response matrix between parton and charged jets. Top right: Corrections factors from parton to charged jets. Lower left: Parton level spectrum with systematic uncertainties. Lower right: NLO charged jet spectra.

14 V0 Feeddown Contributions

Figure 25 shows the total event p_T from PYTHIA simulations for all particles (black), particles with dca < 1 cm (blue), as used in the analysis, and for only primary particles (red). The difference between primary particles and particles with dca < 1 cm is very small. In the analysis we do not correct for the effect since it it much smaller than other systematics.

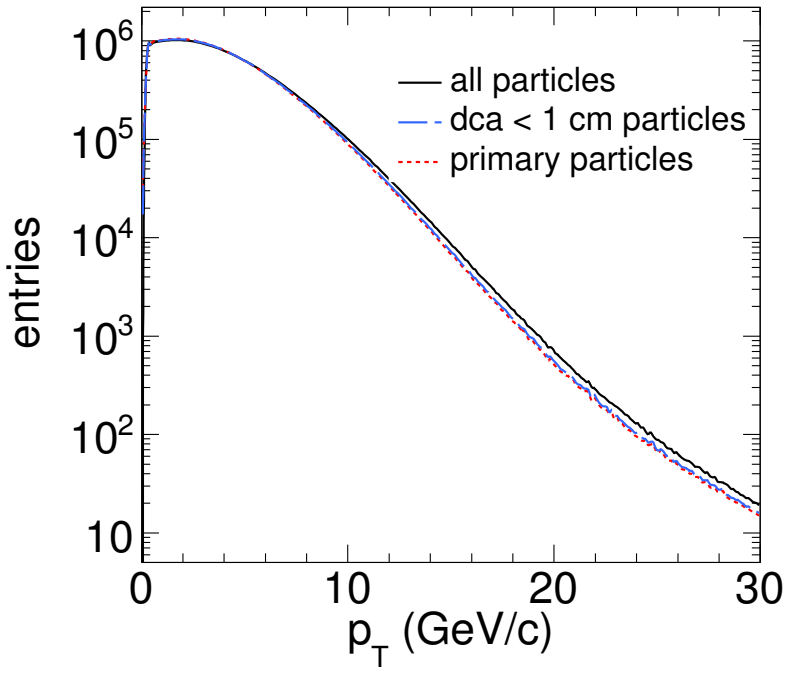

Figure 25: Total event p_T from PYTHIA simulations for all particles (black), particles with dca < 1 cm (blue), as used in the analysis, and for only primary particles (red).